Photoacoustics 31 (2023) 100500

Contents lists available at ScienceDirect

Photoacoustics

journal homepage: www.elsevier.com/locate/pacs

pH-responsive ratiometric photoacoustic imaging of polyaniline nanoparticle-coated needle for targeted cancer biopsy

Ayoung Choe [a,b], David Qin [a], Anthony M. Yu [a], Euisuk Chung [b], Anamik Jhunjhunwala [a], Julian A. Rose [a], Stanislav Y. Emelianov [a,b,*]

[a] Wallace H. Coulter Department of Biomedical Engineering, Georgia Institute of Technology and Emory University School of Medicine, Atlanta, GA 30332, USA
[b] School of Electrical and Computer Engineering, Georgia Institute of Technology, Atlanta, GA 30332, USA

ARTICLE INFO

Keywords:
Polyaniline nanoparticles
Photoacoustic contrast agents
PH sensors
Ratiometric analysis

ABSTRACT

Cancer microenvironment exhibits lower pH compared to healthy tissues, a characteristic which can be exploited using a pH-responsive needle to increase the accuracy of cancer biopsy. A needle, coated with pH-responsive polyaniline (PANI) nanoparticles (PANI-needle), is developed for the minimally invasive and quantitative pH analysis of tissue based on ratiometric photoacoustic (PA) imaging. The ratiometric PA signal from the PANI-needle within the 850–700 nm wavelength range shows a linear response as pH changes from 7.5 to 6.5. Owing to the high surface area of nanostructured PANI, the PA signal of PANI-needle exhibits a fast and reversible response of less than a few seconds. In a tissue-mimicking hydrogel phantom composed of two regions with different pH, PA ratios of PANI-needle successfully differentiate the local pH. The PANI-needle coupled with ultrasound-guided PA imaging is a promising technology for detection of malignant tissue through quantitative pH analysis during needle biopsy.

1. Introduction

For cancer diagnosis, needle biopsies have been widely used to determine the presence of malignant cells within a suspicious area. However, cancer biopsies have a critical limitation of missing the target region resulting in false negatives and multiple biopsy sessions [1]. Ultrasound (US) imaging can increase the accuracy of needle biopsies by guiding the needle to the target region and by providing diagnostic information [2]. Compared to other imaging modalities such as computerized tomography (CT) [3] and positron emission tomography (PET) [4], US imaging has the outstanding advantage of real-time imaging without harmful ionizing radiation [5]. Although US imaging improves needle biopsies substantially, it is still limited by poor tissue contrast and a lack of functional information about the malignancy of lesions, leading to difficulties in detecting tumors and their boundaries [6,7]. For example, within approximately one million prostate biopsies performed in the United States annually, false-negative rates are 20–30% [8,9] leading to possible biopsy repeat and a missed opportunity to treat the cancer in the early stage.

Image-guided needle biopsies could be further improved by using cancer tissue-targeted imaging methods. Integration of biopsy needles with physical or chemical sensors enables more accurate detection of cancer tissues because the needle is in direct contact with the tissue during the insertion. For example, a biopsy needle with an electrical impedance spectroscopy sensor showed a larger impedance for prostate cancer tissues than that of benign tissues [10]. However, the study noted that the electrical property of tissues is also affected by blood flow, cellular metabolism, temperature, and physical hydration level, and therefore, the sensor requires complex calibration for an accurate measurement. A biopsy needle sensor including photonic crystal fibers detected various biomarkers related to cancer cells based on surface-enhanced Raman scattering measurements, however, the approach is limited to liquid biopsies and cannot be used for solid tumors [11]. A multimodal sensor array was also integrated with a biopsy needle for the detection of electrical conductivity, pH, and glucose concentration [12], but the fabrication of a physical/chemical sensor array on the small surface of the needle requires a sophisticated photolithography-based method.

One of the key characteristics of the cancer microenvironment is a relatively low pH caused by the accumulation of lactic acid from the

* Corresponding author at: Wallace H. Coulter Department of Biomedical Engineering, Georgia Institute of Technology and Emory University School of Medicine, Atlanta, GA 30332, USA.
E-mail address: stas@gatech.edu (S.Y. Emelianov).

https://doi.org/10.1016/j.pacs.2023.100500
Received 8 February 2023; Received in revised form 6 March 2023; Accepted 24 April 2023
Available online 26 April 2023
2213-5979/© 2023 Published by Elsevier GmbH. This is an open access article under the CC BY-NC-ND license (http://creativecommons.org/licenses/by-nc-nd/4.0/).

high glycolytic activity of cancer cells [13–15]. While indicative of cancer cell presence, the pH level may also provide information about the proliferation and aggressiveness of cancer cells [16,17]. Efforts have been made to detect the deep-tissue pH in the cancer microenvironment through measurement of pH-responsive fluorescence in the second near-infrared window (NIR-II), however, NIR-II fluorophores suffer from low quantum yield and extinction coefficient, and reduced photostability [18,19]. Miniaturized pH electrodes for local pH detection were also explored but pH electrodes require pre-calibration [20,21]. Using tissue-mimicking hydrogel phantom, it was shown that pH sensor integrated with a biopsy needle can distinguish cancer from normal tissue, the fabrication process required sophisticated deposition of electrodes and sensing materials [12]. Therefore, it is desired to develop a simply fabricated sensor to measure the local pH level of the tissue, improving the accuracy of cancer biopsies.

To meet the challenge, we used polyaniline (PANI), a conducting polymer that has pH-responsive light absorption properties in the near-infrared (NIR) region, good biocompatibility, and excellent environmental stability [22]. Using human cell lines, previous studies have shown great biocompatibility and low toxicity of PANI nanostructures [23–25]. The molecular structure of PANI shifts from an emeraldine base (EB) to an emeraldine salt (ES) state in acidic environments, leading to a shift of its absorption peak to a longer wavelength [26]. Owing to its pH-sensitive light absorption and high biocompatibility, PANI has often been used as a photoacoustic (PA) contrast agent in conjunction with gold nanoparticles [27], bovine serum albumin [28], or iron-copper [29] to image gastric dysfunction or cancer tissues. The use of PA imaging enables deep-tissue pH detection, which is attributed to the low attenuation of sound waves as they propagate through tissue [30]. For the biomedical application,

In this study, we developed a highly sensitive biopsy needle coating based on pH-responsive PANI nanoparticles (NPs) which can display a change in PA ratiometric signal within the cancer microenvironment. The ratiometric PA analysis showed great performance in the quantitative measurement of pH surrounding the PANI NPs-coated needle (PANI-needle) without complex pre-calibration. Additionally, the PANI-needle had rapid and reversible responses to cyclic pH changes and showed accurate determination of pH when inserted into a tissue-mimicking hydrogel phantom. The US-guided PA imaging of PANI-needle represents a promising approach to increase the accuracy of cancer biopsies.

2. Materials and methods

2.1. Materials

Aniline, ammonium persulfate (APS), dopamine hydrochloride (DA), hydrochloric acid (HCl), sodium hydroxide (NaOH), acrylamide (AAm), N,N′-methylenebisacrylamide (BIS), and isopropyl alcohol (IPA) were purchased from Sigma-Aldrich (MO, USA). Phosphate buffered saline (PBS) was purchased from VWR Chemicals (PA, USA), and N,N,N′,N′-Tetramethylethylenediamine (TEMED) was purchased from Beantown Chemical (NH, USA). The chemical compounds were used as received without further purification. Sandpapers were purchased from 3 M (401Q Imperial Wetordry, 1000 grit).

2.2. Synthesis of PANI NPs

PANI NPs were synthesized using chemical oxidative polymerization of aniline using APS without mechanical stirring [31]. Aniline monomer solution was prepared by adding aniline (50 μL) to HCl (1 M, 5 mL) solution. Then, APS aqueous solution (0.02 g mL^{-1}) was added, dropwise, to the aniline solution, and the reaction continued for 24 h. The PANI NPs were collected and washed by centrifuge (10000 rpm, 30 min) and redispersion in deionized (D.I.) water 3 times.

2.3. Fabrication of PANI-needles

The PDA-coated needles were prepared using oxidated self-polymerization of DA in an alkaline condition [32]. 30-gauge stainless-steel needles were washed by sonication for 10 min and dried with nitrogen gas. The needles were immersed into PBS solution (pH 8.5) containing DA (2 mg mL^{-1}). The pH level was adjusted by adding NaOH and measured using a pH meter (Orion Star A215, Thermo Scientific, USA). The reaction was done at room temperature with magnetic stirring for 24 h, and the PDA-coated needles were washed with D.I. water and dried with nitrogen gas. The PANI dispersion was then drop-casted onto the PDA-coated needle, and the PANI dispersion (160 μL) was used for each needle.

2.4. Preparation of hydrogel phantoms

The pH of PBS buffer solution was adjusted by adding an appropriate amount of HCl or NaOH solution to the PBS buffer solution, and the adjusted pH level was measured using a pH meter. The cancer tissue-mimicking hydrogel phantom was prepared using a PAAm hydrogel and the PBS buffer solution with adjusted pH level. The APS solution in PBS (200 μL, 100 mg mL^{-1}) was added to the mixture of AAm (1.9 g), BIS (0.1 g), and PBS solution (18.231 mL), and 7 mL of the solution was poured into a silicone mold ($2 \times 2 \times 2$ cm^3). The air bubbles were removed using a vacuum chamber for 60 s, and polymerization was started by adding TEMED (8.75 μL). After 20 min, the PAAm hydrogel was detached from the mold and immersed in the PBS solution with adjusted pH level before the measurement to stabilize the pH level and prevent drying of the solvent.

2.5. Characterization of PANI NPs

The morphology of PANI NPs was observed using a scanning electron microscope (SEM, SU8230, Hitachi, Tokyo, Japan). To reduce electron charging on the sample surface, Au sputtering (Hummer 6 sputter coater, USA) was performed with 30 mA for 60 s. The light absorption spectra of PANI dispersions were measured using a UV-Vis-NIR spectrophotometer (Evolution 220, Thermo Scientific, MA, USA). The Raman spectra of PANI- and PDA-coated needles, and PANI-needle were measured using a confocal Raman microscope (Renishaw, UK). The Raman spectra were obtained using 5 accumulations, 10 s of integration time, and 0.064 mW intensity of 488 nm laser source.

2.6. US/PA imaging of PANI dispersions and PANI-needles

A tube phantom was prepared using polyethylene tubes (1.14 mm inner diameter, 1.63 mm outer diameter) fixed in a 3D-printed frame. For the US/PA imaging of PANI dispersions, each tube contained 35 μL of PANI dispersion. The US/PA images were obtained using a Vevo 2100/LAZR imaging system (FujiFilm VisualSonics, Toronto, Canada). The system was operated with an LZ250 US transducer (fc = 21 MHz) with integrated fiber optic light delivery. Laser was generated from a Q-switched Nd:YAG laser (1064 nm) pumping an optical parametric oscillator (OPO), giving a 7 ns pulse width and a 10 Hz pulse repetition frequency. The PA spectra of PANI were obtained using the OPO wavelength range from 700 to 950 nm at 5 nm interval. The PA data were processed using VevoLAB 2.2 and MATLAB R2021a (Mathworks, USA). For the US/PA imaging of PANI-needles, each tube had 35 μL of pH-adjusted PBS solution, and the PANI-needles were placed inside the tubes. For the preparation of the hydrogel phantom with two different pH levels, two PAAm hydrogels were wrapped with a parafilm (Bemis, USA) to block the diffusion of the different pH solutions.

3. Results and discussion

As a nanosecond laser pulse irradiates the PANI-needle inserted into

tissue, PANI NPs absorb the incident light to generate PA signals depending on the surrounding pH (Fig. 1a, left). Acidic conditions induce the increase and decrease of PA signals at 850 nm (PA_{850}) and 700 nm (PA_{700}), respectively (Fig. 1a, right) thus enabling the detection of tumor tissues based on the analysis of PA_{850}/PA_{700} ratio in real time. The ratiometric PA imaging allows an accurate detection of pH surrounding the PANI-needle by eliminating the interference caused by the unstable excitation intensity [33]. The scanning electron microscopy (SEM) images show the PANI-needle having uniformly coated PANI NPs and short fibrous morphology of PANI NPs (Fig. 1b-c).

The extracellular pH of tissues in the human body is approximately 7.5, decreasing in cancer microenvironments to as low as 6.5 [15]. According to the established pH range of healthy and cancerous tissues, the light absorption spectra of PANI NP dispersions (PANI dispersions) prepared with pH-adjusted phosphate buffered saline (PBS) solutions were analyzed from pH 6.5–7.5 at intervals of 0.25 (Fig. 2a). When pH was decreased from 7.5 to 6.5, the light absorption peak at approximately 700 nm gradually shifted to 850 nm, indicating the change of molecular structure of PANI from the EB to ES state [26]. When comparing the absorbance intensities at 700 and 850 nm wavelengths as pH is reduced from 7.5 to 6.5, the intensity at 700 nm linearly decreases from 0.67 to 0.63 while the intensity at 850 nm linearly increases from 0.56 to 0.69 (Fig. 2b). Therefore, the absorbance ratio of 850–700 nm linearly increases by 31% from 0.83 to 1.09 when pH is decreased from 7.5 to 6.5 (Fig. S1).

The PA response of PANI NPs to pH changes was first evaluated in the dispersion state. For US-guided PA (US/PA) imaging, PANI dispersions at different pH levels were prepared and placed inside of the polyethylene (PE) tubes fixed in a 3D-printed frame (Fig. S2). The pH-responsive US/PA images of PANI dispersions at 700 and 850 nm pulsed laser wavelengths are shown in Fig. 2c (i) and (ii), respectively. The noticeable PA intensity of PANI dispersion compared with that of water reference is attributed to the great light absorption property of PANI NPs. In particular, Fig. 2c (iii) displays a gradual increase of the intensity of PA_{850}/PA_{700} as pH is decreased from 7.5 to 6.5. The PA ratio values also showed a linear increase with a sensitivity of 0.21 pH^{-1} and a high R-Squared value of 0.98 as pH is decreased from 7.5 to 6.5 (Fig. 2d). The PA ratio values were calculated from the PA spectra of PANI dispersions at different pH levels (Fig. S3). In the PA spectra of PANI dispersions, the signal intensity at longer wavelengths gradually decreased as the pH was reduced, which is well-correlated to the pH-dependent change in light absorption spectra shown in Fig. 2a.

To maximize the sensitivity to pH changes, the wavelengths used for the absorbance and PA ratios were empirically selected as 700 and 850 nm. The light absorption peak of PANI dispersion shifts from 700 to 850 nm as the pH is reduced from 7.5 to 6.5 (Fig. 2a). The slope of PA_{850}/PA_{700} with respect to pH was higher than that of PA_{800}/PA_{700} and PA_{900}/PA_{700}, indicating the former wavelength pair is the most sensitive to pH changes (Fig. S4). For future in vivo experiments, however, the effect of tissue scattering may require further adjustment of the selected wavelengths [34].

As described in the Experimental Section, the pH-responsive PANI-needle was fabricated using the PDA-coated needle prepared by in-situ oxidative self-polymerization of dopamine on the stainless-steel needle. The PDA layer improves homogeneity of PANI coating based on the strong adhesive force of amine and catechol groups in the PDA molecule and the π-π interaction between PDA and PANI molecules (Fig. 3a). Compared to a PANI NPs-coated bare needle, the PANI-needle prepared with the PDA-coated needle had a more uniform PANI layer (Fig. S5). The PA intensity of the PANI-needle was observed through US/PA imaging compared to the bare and PDA-coated needles at 700 nm under the same pH level (Fig. 3b). Owing to the great light absorption property of PANI NPs, the average PA intensity of the PANI-needle was 3.07 and 1.86 times higher than those of the bare and PDA-coated needles, respectively (Fig. S6). Moreover, the homogeneity of coated PANI NPs was analyzed using the US/PA image of PANI NPs coated on bare, sanded, and PDA-coated needles. The rough surface of a sanded needle can increase the surface hydrophilicity due to an increase in the overall surface area [35], decreasing the contact angle of aqueous PANI dispersion. Nevertheless, the PDA layer remained the most effective method to obtain a homogeneous PANI coating as the PANI-needle prepared with the PDA-coated needle showed more uniform and

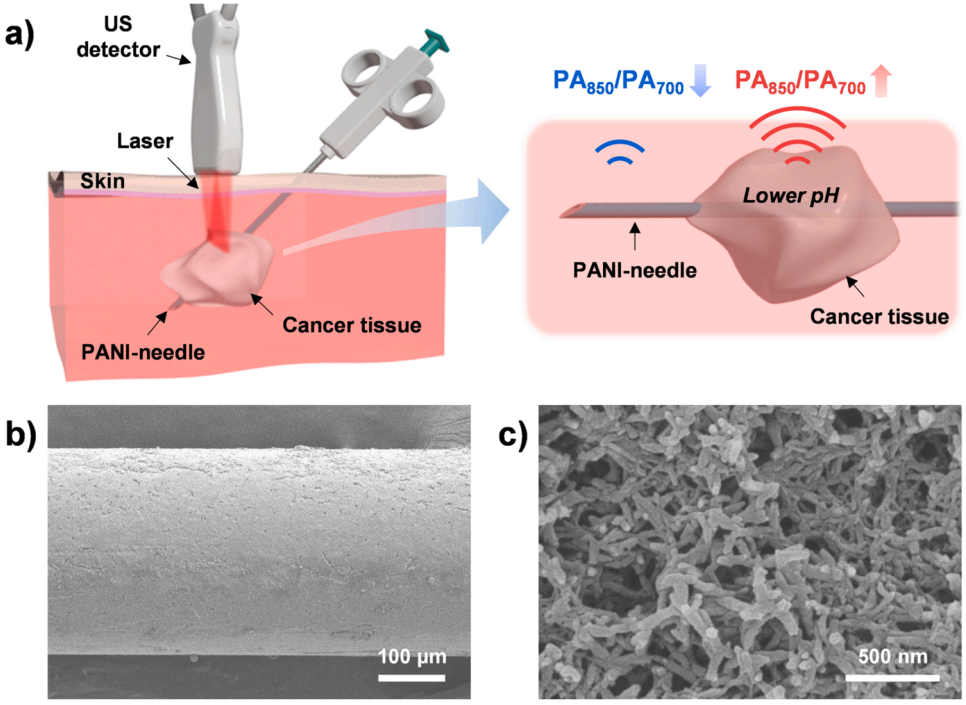

Fig. 1. Imaging of the cancer tissue using a needle coated by pH-responsive polyaniline nanoparticles (PANI NPs). (a) Scheme of ultrasound-guided photoacoustic (US/PA) imaging of PANI NPs-coated needle (PANI-needle). PA_{850}/PA_{700} denotes the PA ratio of 850–700 nm. Scanning electron microscopy (SEM) images of (b) the PANI-needle and (c) PANI NPs coated on the needle.

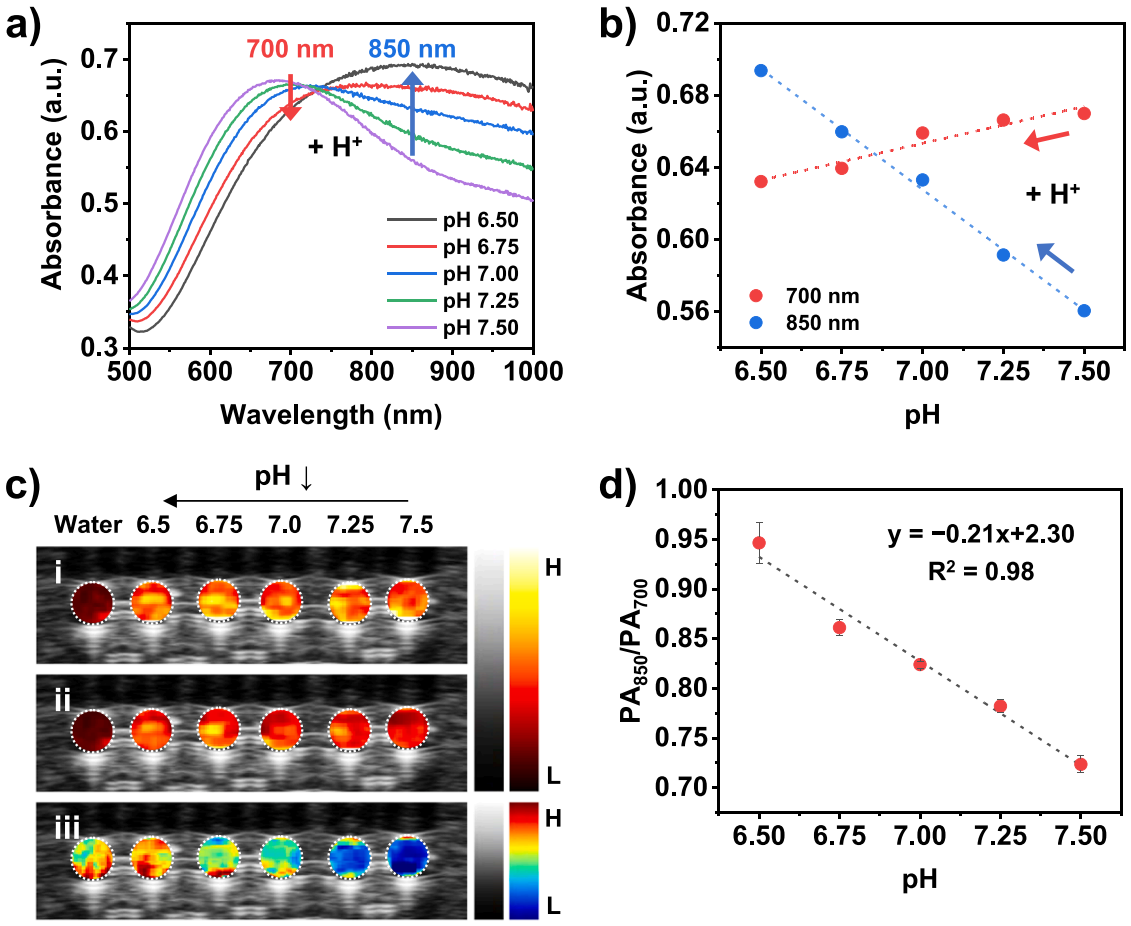

Fig. 2. pH-responsive optical and PA properties of PANI dispersions. (a) UV–vis spectra of PANI dispersions at different pH levels. (b) pH-dependent absorbance change of the PANI dispersion at wavelengths of 700 and 850 nm. (c) US/PA images of water and PANI dispersions prepared with different pH solutions at (i) 700 nm, (ii) 850 nm, and (iii) US image-combined ratiometric PA image of 850–700 nm. PA images were segmented to show regions of interest. (d) pH-dependent change of the PA ratio for PANI dispersions. Dotted lines of (b) and (d) denote linear fits. Error bars in (d) denote standard deviation from three different samples.

higher PA intensity compared to PANI-needles which were prepared using bare and sanded needles (Fig. S7).

The homogeneous coating of PANI is attributed to the PDA layer on the needle, inducing π-π stacking interaction between PANI and PDA molecules. To analyze the interaction between PANI and PDA molecules, the Raman spectra were observed for the PANI-coated, PDA-coated, and PANI-PDA-coated needles (Fig. S8). The PANI-coated needle had representative maximum peaks at 1617 and 1491 cm^{-1} for the C═C and C═N stretching vibration of quinonoid rings, respectively [36]. For the PANI-PDA-coated needle, the peak of C═C stretching vibration slightly shifted to 1621 cm^{-1} due to the π-π interactions between the benzene rings of PANI and the catechol groups of PDA [37]. Additionally, by comparing the relative intensity of C═C bond compared to that of C═N bonds in quinonoid units, the PANI-PDA-coated needle showed higher relative intensity for the C═C stretching vibration peak than the PANI-coated needle, proving the existence of PDA which has a broad Raman peak at 1580 cm^{-1} from the stretching vibration of aromatic rings [38].

Fig. 3c exhibits the PA spectra of PANI-needles prepared with PDA-coating for pH levels between 6.5 and 7.5 at intervals of 0.25. As the pH was decreased, the PA intensity at the longer wavelength increased, caused by the pH-responsive shift of the light absorption peak (Fig. 2a, b). The pH-dependent PA ratio was calculated from the PA spectra; the PA ratio linearly increased with a sensitivity of 0.24 pH^{-1} as the pH was decreased (Fig. 3d). The sensitivity of the PANI-needle was similar to that of the PANI dispersion due to strong light absorption properties of PANI NPs. Next, the ratiometric PA images of the PANI-needles were obtained over the pH range of 6.5–7.5 using the PA images at 700 and 850 nm (Fig. S9). Similar to the pH-dependent PA ratio of PANI dispersion, the highest and lowest intensities of the PA ratio were measured at pH 6.5 and 7.5, respectively, and a gradual increase in the PA ratio intensity was also observed as the pH was decreased from 7.5 to 6.5.

The pH measurement performed by imaging the needle in the target region must be rapid because the cancer biopsy is performed within 15–30 s [39]. To assess the response time of the PANI-needle, real-time monitoring of the PA signal at a single laser wavelength of 850 nm was observed while changing the pH level. As shown in Fig. 4a, the PANI-needle was placed inside the PE tube filled with the pH solution and the pH level was changed by injecting the different pH solution. The response time was defined based on the time required for the PANI-needle to reach 90% of its saturated PA intensity during both the response and recovery processes [40]. The pH level surrounding the PANI-needle was changed from 7.5 to 6.5 by quickly injecting the pH 6.5 solution into the PE tube at approximately 60 s, followed by a re-injection of pH 7.5 solution at around 125 s to recover the original pH level (Fig. 4b). As a result, the PA intensity quickly increased and saturated after the injection of pH 6.5 solution and successfully recovered to the original level after injecting pH 7.5 solution. The response and recovery times were 3.95 and 5.53 s, respectively, demonstrating rapid responses of PA signal to sudden pH changes which may occur as the needle passes through a cancerous tissue during a biopsy. The rapid response to pH changes is due to the large surface area of the nanostructured PANI layer [22]. The reversible changes of pH-dependent PA

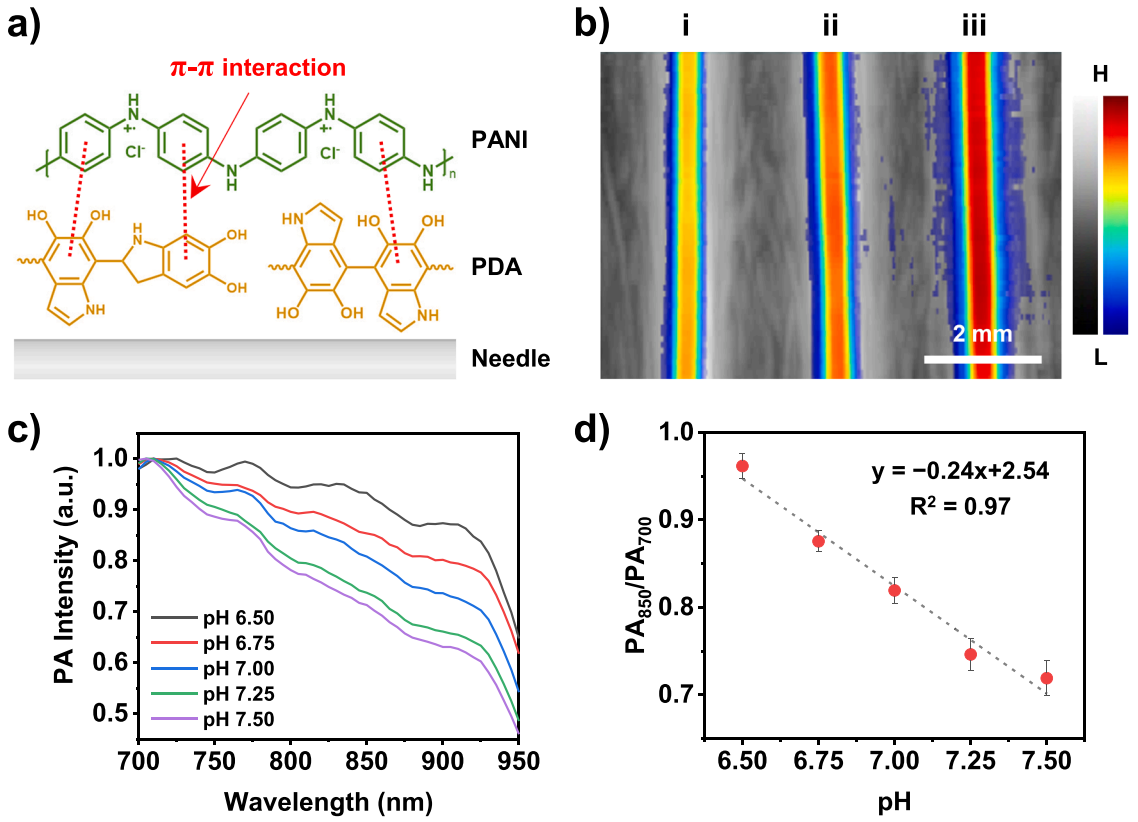

Fig. 3. pH-responsive PA analysis of the PANI-needle. (a) Schematic illustration of the interaction between PANI and polydopamine (PDA) molecules on the needle surface. (b) US/PA image of the (i) bare needle, (ii) PDA-needle, and (iii) PANI-needle at 700 nm. (c) PA spectra of PANI-needles at different pH levels. The PA spectra were normalized by the maximum value of each plot and a moving average filter (n = 5) was applied. (d) pH-dependent change of the PA ratio for the PANI-needle. The dotted line is the linear fit of the data. Error bars in (d) denote standard deviation from three different samples.

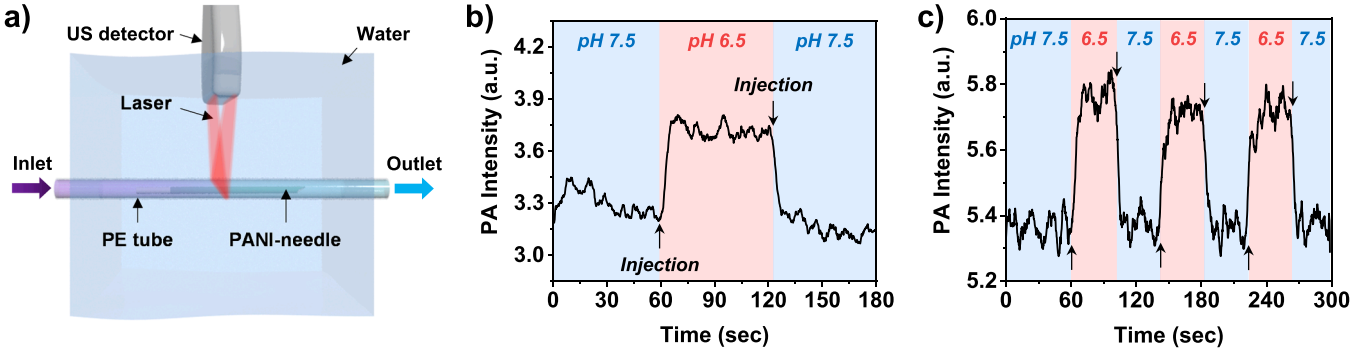

Fig. 4. Dynamic response of the PA signal from the PANI-needle as pH changes. (a) Scheme of the real-time PA measurement of the PANI-needle while changing the pH level. (b) Time-dependent PA intensity of the PANI-needle at 850 nm laser wavelength. The pH level was changed from 7.5 to 6.5 at 60 s and from 6.5–7.5 at 125 s. The injection of pH solution took around 1 s (c) The reversible changes in PA intensity of the PANI-needle during cyclic changes in pH. A moving average filter (n = 19) was applied to the time-dependent PA intensity plots. The arrows indicate the injection time of different pH solutions.

signal were also stable during 3 cyclic changes of pH between 7.5 and 6.5 (Fig. 4c).

The pH-sensing ability of the PANI-needle was also validated using a tissue-mimicking polyacrylamide (PAAm) hydrogel phantom consisting of two PAAm hydrogel blocks at different pH levels, pH 6.5 and 7.5 (Fig. 5a). The PAAm blocks were fabricated through crosslinking polymerization of acrylamide in the pH-adjusted PBS solution. For the US/PA imaging, the two blocks were placed next to each other, with the interface between the blocks separated by a parafilm to prevent the diffusion of the different pH solutions. The PANI-needle was inserted in the hydrogel phantom, passing through both hydrogel blocks. Fig. 5b (i) shows the top-view US image of the PANI-needle in the hydrogel phantom, and Fig. 5b (ii) and (iii) shows top-view PA images at 700 and 850 nm wavelengths, respectively. Using the PA images at two different wavelengths, the ratiometric PA image of 850–700 nm was calculated (Fig. 5b (iv)). As a result, the calculated ratiometric PA image showed higher PA_{850}/PA_{700} intensity in the pH 6.5 hydrogel, a result well-correlated with previously observed trends. Considering clinical US-guided biopsies which have flexible imaging orientations, the ratiometric PA signal of PANI-needle should be observable and consistent in different views such as coronal or sagittal to navigate situations where the signal is impeded by bones or air pockets. For the same PANI-needle inserted in the hydrogel phantom of Fig. 5b, the side-view ratiometric PA image also showed higher values in the pH 6.5 hydrogel compared to

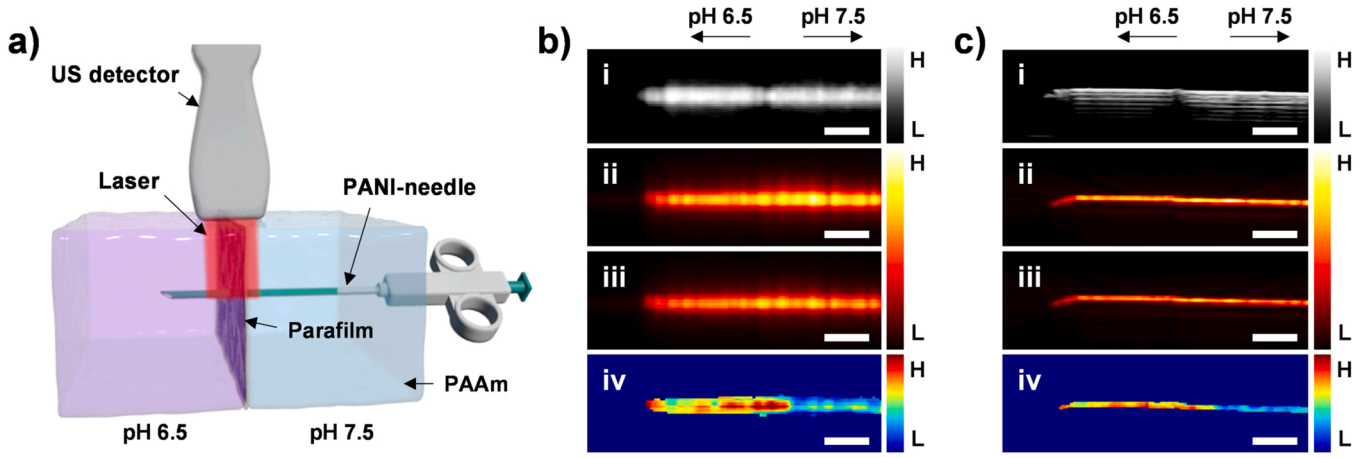

Fig. 5. PA imaging of the PANI-needle in the hydrogel phantom prepared with two different pH solutions, 6.5 and 7.5. (a) Scheme of US/PA imaging PANI-needle in the hydrogel phantom at different pH levels. US/PA images of PANI-needle in (b) top view and (c) side view for (i) US images, PA images at (ii) 700 nm, (iii) 850 nm, and (iv) 850 nm/700 nm ratiometric PA images. Scale bars: 2 mm.

the pH 7.5 hydrogel, providing consistency of pH-dependent ratiometric PA imaging (Fig. 5c). The ratiometric PA images demonstrate that the PANI-needle successfully detects the surrounding pH level of a tissue-mimicking environment in different views.

4. Conclusion

In conclusion, the pH-responsive biopsy needle coated with PANI NPs was successfully fabricated for PA imaging of tissue pH. The adhesion of PANI NPs to the needle was improved by coating the needle with PDA taking advantage of the π-π interaction between the benzene rings of PANI and the catechol groups of PDA. The pH-dependent PA signal amplitude ratio showed a linear increase with a sensitivity of 0.24 pH^{-1} as pH decreased from 7.5 to 6.5. Due to the high surface area of the nanostructured PANI layer, the PANI-needle had a fast response time of less than 4 s during pH changes. The pH-responsive change in PA intensity was also shown to be reversible, which is crucial for detecting whether the PANI-needle has reached cancerous tissue or has missed or traversed through the lesion. The PANI-needle also successfully detected the pH difference in a tissue-mimicking hydrogel phantom based on ratiometric PA images. Overall, our study suggests that ratiometric PA imaging of the pH-responsive PANI-needle can be used to measure the pH of suspicious tissues.

Declaration of Competing Interest

The authors declare that they have no known competing financial interests or personal relationships that could have appeared to influence the work reported in this paper.

Data availability

Data will be made available on request.

Acknowledgements

This work was supported by the Breast Cancer Research Foundation (BCRF-22–043) and National Institute of Health (EB028916 and NS117613).

Appendix A. Supporting information

Supplementary data associated with this article can be found in the online version at doi:10.1016/j.pacs.2023.100500.

References

[1] R. Kumar, R. Srivastava, S. Srivastava, Detection and classification of cancer from microscopic biopsy images using clinically significant and biologically interpretable features, J. Med. Eng. 2015 (2015), 457906.
[2] A.A. Bhatt, D.H. Whaley, C.U. Lee, Ultrasound-guided breast biopsies: basic and new techniques, J. Med. Ultrasound 40 (2021) 1427–1443.
[3] L.H. d O. Schiavon, C.J. Tyng, D.J. Travesso, R.D. Rocha, A.C.S.A. Schiavon, A.G. V. Bitencourt, Computed tomography-guided percutaneous biopsy of abdominal lesions: indications, techniques, results, and complications, Radiol. Bras. 51 (2018) 141–146.
[4] B. Fei, D.M. Schuster, PET molecular imaging–directed biopsy: a review, AJR Am. J. Roentgenol. 209 (2017) 255.
[5] P.N. Wells, Ultrasound imaging, Phys. Med. Biol. 51 (2006) R83.
[6] A.M. Wallace, C. Comstock, C.K. Hoh, D.R. Vera, Breast imaging: a surgeon's prospective, Nucl. Med. Biol. 32 (2005) 781–792.
[7] Q. Huang, Y. Luo, Q. Zhang, Breast ultrasound image segmentation: a survey, Int. J. Comput. Assist. Radiol. Surg. 12 (2017) 493–507.
[8] M. Dimmen, L. Vlatkovic, K.H. Hole, J.M. Nesland, B. Brennhovd, K. Axcrona, Transperineal prostate biopsy detects significant cancer in patients with elevated prostate-specific antigen (PSA) levels and previous negative transrectal biopsies, BJU Int 110 (2012) E69–E75.
[9] J.G. Rivas, M. Alvarez-Maestro, M. Czarniecki, S. Czarniecki, M.R. Socarras, S. Loeb, Negative biopsies with rising prostate-specific antigen. What to do? EMJ Urol. 5 (2017) 76–82.
[10] V. Mishra, H. Bouayad, A. Schned, A. Hartov, J. Heaney, R.J. Halter, A real-time electrical impedance sensing biopsy needle, Ieee. Trans. Biomed. Eng. 59 (2012) 3327–3336.
[11] U. Dinish, F. Beffara, G. Humbert, J.L. Auguste, M. Olivo, Surface-enhanced Raman scattering-active photonic crystal fiber probe: towards next generation liquid biopsy sensor with ultra high sensitivity, J. Biophotonics 12 (2019), e201900027.
[12] J. Park, Y. Jeong, J. Kim, J. Gu, J. Wang, I. Park, Biopsy needle integrated with multi-modal physical/chemical sensor array, Biosens. Bioelectron. 148 (2020), 111822.
[13] O. Warburg, F. Wind, E. Negelein, The metabolism of tumors in the body, J. Gen. Physiol. 8 (1927) 519–530.
[14] Y. Kato, S. Ozawa, C. Miyamoto, Y. Maehata, A. Suzuki, T. Maeda, Y. Baba, Acidic extracellular microenvironment and cancer, Cancer Cell Int 13 (2013) 89.
[15] G. Hao, Z.P. Xu, L. Li, Manipulating extracellular tumour pH: an effective target for cancer therapy, RSC Adv. 8 (2018) 22182–22192.
[16] J.S. Fang, R.D. Gillies, R.A. Gatenby, Adaptation to hypoxia and acidosis in carcinogenesis and tumor progression, Semin. Cancer Biol. 18 (2008) 330–337.
[17] S. Lee, A. Shanti, Effect of exogenous pH on cell growth of breast cancer cells, Int. J. Mol. Sci. 22 (2021) 9910.
[18] C. Li, G. Chen, Y. Zhang, F. Wu, Q. Wang, Advanced fluorescence imaging technology in the near-infrared-II window for biomedical applications, J. Am. Chem. Soc. 142 (2020) 14789–14804.
[19] Z. Lei, F. Zhang, Molecular engineering of NIR-II fluorophores for improved biomedical detection, Angew. Chem. Int. Ed. 60 (2021) 16294–16308.
[20] J.J. García-Guzmán, C. Pérez-Ràfols, M. Cuartero, G.A. Crespo, Toward in vivo transdermal pH sensing with a validated microneedle membrane electrode, ACS Sens 6 (2021) 1129–1137.
[21] S. Dulay, L. Rivas, S. Miserere, L. Pla, S. Berdún, J. Parra, E. Eixarch, E. Gratacós, M. Illa, M. Mir, In vivo monitoring with micro-implantable hypoxia sensor based on tissue acidosis, Talanta 226 (2021), 122045.
[22] N. Abu-Thabit, Y. Umar, E. Ratemi, A. Ahmad, F. Ahmad, Abuilaiwi, A flexible optical pH sensor based on polysulfone membranes coated with pH-responsive polyaniline nanofibers, Sensors 16 (2016) 986.

[23] E.N. Zare, P. Makvandi, B. Ashtari, F. Rossi, A. Motahari, G. Perale, Progress in conductive polyaniline-based nanocomposites for biomedical applications: a review, J. Med. Chem. 63 (2019) 1–22.
[24] P. Villalba, M.K. Ram, H. Gomez, V. Bhethanabotla, M.N. Helms, A. Kumar, A. Kumar, Cellular and in vitro toxicity of nanodiamond-polyaniline composites in mammalian and bacterial cell, Mater. Sci. Eng. C. 32 (2012) 594–598.
[25] Z. Kucekova, P. Humpolicek, V. Kasparkova, T. Perecko, M. Lehocký, I. Hauerlandova, P. Saha, J. Stejskal, Colloidal polyaniline dispersions: antibacterial activity, cytotoxicity and neutrophil oxidative burst, Colloids Surf. B 116 (2014) 411–417.
[26] P. Kong, P. Liu, Z. Ge, H. Tan, L. Pei, J. Wang, P. Zhu, X. Gu, Z. Zheng, Z. Li, Conjugated HCl-doped polyaniline for photocatalytic oxidative coupling of amines under visible light, Catal. Sci. Technol. 9 (2019) 753–761.
[27] W. Huang, R. Chen, Y. Peng, F. Duan, Y. Huang, W. Guo, X. Chen, L. Nie, In vivo quantitative photoacoustic diagnosis of gastric and intestinal dysfunctions with a broad pH-responsive sensor, ACS Nano 13 (2019) 9561–9570.
[28] Q. Tian, Y. Li, S. Jiang, L. An, J. Lin, H. Wu, P. Huang, S. Yang, Tumor pH-responsive albumin/polyaniline assemblies for amplified photoacoustic imaging and augmented photothermal therapy, Small 15 (2019) 1902926.
[29] S. Wang, L. Zhang, J. Zhao, M. He, Y. Huang, S. Zhao, A tumor microenvironment–induced absorption red-shifted polymer nanoparticle for simultaneously activated photoacoustic imaging and photothermal therapy, Sci. Adv. 7 (2021) eabe3588.
[30] Z. Zhao, C.B. Swartchick, J. Chan, Targeted contrast agents and activatable probes for photoacoustic imaging of cancer, Chem. Soc. Rev. 51 (2022) 829–868.
[31] J. Tan, Z. Xie, Z. Zhang, Y. Sun, W. Shi, D. Ge, Dopamine modified polyaniline with improved adhesion, dispersibility, and biocompatibility, J. Mater. Sci. 53 (2018) 447–455.
[32] Y. Zhao, R. Liu, Y. Fan, B. Zhao, W. Qian, J. Guo, C. Li, S. Chen, G. Luo, H. Deng, J. Zhang, Self-sealing hemostatic and antibacterial needles by polyphenol-assisted surface self-assembly of multifunctional nanoparticles, Chem. Eng. J. 425 (2021), 130621.
[33] C. Zhang, Z. Qiu, L. Zhang, Q. Pang, Z. Yang, J.-K. Qin, H. Liang, S. Zhao, Design and synthesis of a ratiometric photoacoustic imaging probe activated by selenol for visual monitoring of pathological progression of autoimmune hepatitis, Chem. Sci. 12 (2021) 4883–4888.
[34] S.L. Jacques, Optical properties of biological tissues: a review, Phys. Med. Biol. 58 (2013) R37.
[35] R.N. Wenzel, Resistance of solid surfaces to wetting by water, Ind. Eng. Chem. 28 (1936) 988–994.
[36] J. Stejskal, M. Trchová, P. Bober, P. Humpolíček, V. Kašpárková, I. Sapurina, M. A. Shishov, M. Varga, Conducting polymers: polyaniline, Encycl. Polym. Sci. Technol. (2002) 1–44.
[37] X. Chen, J. Zhou, Y. Zhang, S. Zhu, X. Tian, F. Meng, L. Cui, P. Xue, R. Huang, J. Sun, Polydopamine-modified polyaniline/nanodiamond ternary hybrids with brain fold-like surface for enhanced dual band electromagnetic absorption, ACS Appl. Polym. Mater. 1 (2019) 405–413.
[38] B. Fei, B. Qian, Z. Yang, R. Wang, W. Liu, C. Mak, J.H. Xin, Coating carbon nanotubes by spontaneous oxidative polymerization of dopamine, Carbon 46 (2008) 1795–1797.
[39] J.C. Crockett, The thyroid nodule: fine-needle aspiration biopsy technique, J. Med. Ultrasound 30 (2011) 685–694.
[40] M.J. McGrath, C.N. Scanaill, Sensing and sensor fundamentals. Sensor technologies, Springer, 2013, pp. 15–50.

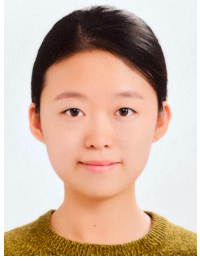

Ayoung Choe: Dr. Ayoung Choe is a postdoctoral researcher in the Wallace H. Coulter Department of Biomedical Engineering and the School of Electrical and Computer Engineering at the Georgia Institute of Technology. She received her Ph.D. degree in Energy Engineering from the Ulsan National Institute of Science and Technology (UNIST), Ulsan, Republic of Korea in 2020. Her research focuses on developing stimuli-responsive nanoparticle-based contrast agents for photoacoustic imaging and their clinical applications.

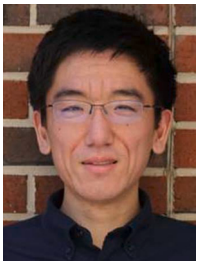

David Qin: David Qin is a graduate student in the Wallace H. Coulter Department of Biomedical Engineering at the Georgia Institute of Technology and Emory University. His research focuses on employing photoacoustic and ultrasound imaging together with nanoparticle contrast agents for pre-clinical science. These include the tracking of endogenous circulating stem cells and immune cells in aged mouse models responding to injury. In addition, he investigates fluence compensation techniques to improve the quantitative accuracy of photoacoustic imaging at depth.

Anthony M. Yu: Anthony Yu is a graduate student in the Wallace H. Coulter Department of Biomedical Engineering at the Georgia Institute of Technology and Emory University. His research focuses on employing tomographic photoacoustic, ultrasound, and fluorescence imaging techniques in combination with nanoagents for a range of diagnostic applications. These include the detection of early metastasis in breast and skin cancers and studying the development of vasculature in response to bioscaffold implantation.

Euisuk Chung: Euisuk Chung is a graduate student in the electrical and computer engineering at the Georgia Institute of Technology. His research mainly focuses on the design and development of contrast agent and imaging techniques with ultrasound and photoacoustic for drug delivery and cancer diagnosis. These include the tracking of contrast agent and measurement released drug dose with ultrasound and photoacoustic imaging.

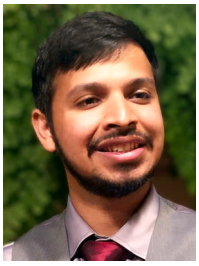

Anamik Jhunjhunwala: Anamik Jhunjhunwala is a graduate student in the Wallace H. Coulter Department of Biomedical Engineering at the Georgia Institute of Technology and Emory University. His research mainly focuses on the design and development of photoacoustic nanosensors for stem cell therapy and immunotherapy. Some examples include plasmonic nanoparticles which monitor stem cell location and viability or photomagnetic nanoparticles for trimodal ultrasound, photoacoustic, and MRI.

Julian A. Rose Julian Rose is a graduate student in the Wallace H. Coulter Department of Biomedical Engineering at the Georgia Institute of Technology and Emory University. His research focuses on the use of photomagnetic contrast agents and targeted laser irradiation to develop an improved small animal model of glaucoma and ultimately explore therapeutic strategies.

Stanislav Y. Emelianov: Dr. Stanislav Emelianov is a Joseph M. Pettit Endowed Chair, Georgia Research Alliance Eminent Scholar, and Professor of Electrical & Computer Engineering and Biomedical Engineering at the Georgia Institute of Technology and Emory University School of Medicine. Furthermore, Dr. Emelianov is Director of the Ultrasound Imaging and Therapeutics Research Laboratory. Projects in Dr. Emelianov's laboratory are focused on the discovery, development, and clinical translation of diagnostic imaging and therapeutic instrumentation, augmented with theranostic nanoagents.